Title
Influence of ENSO and the NAO on terrestrial carbon uptake in the Texas-northern Mexico region

Journal
Global Biogeochemical Cycles, 29(8)

ISSN
0886-6236

Authors
Parazoo, Nicholas C
Barnes, Elizabeth
Worden, John
et al.

Publication Date
2015-08-01

DOI
10.1002/2015gb005125

Peer reviewed

Influence of ENSO and the NAO on terrestrial carbon uptake in the Texas-northern Mexico region

Nicholas C. Parazoo[1,2], Elizabeth Barnes[3], John Worden[1], Anna B. Harper[4], Kevin B. Bowman[1,2], Christian Frankenberg[1], Sebastian Wolf[5,6], Marcy Litvak[7], and Trevor F. Keenan[8]

[1] Jet Propulsion Laboratory, California Institute of Technology, Pasadena, California, USA, [2] Joint Institute for Regional Earth System Science and Engineering, University of California, Los Angeles, California, USA, [3] Department of Atmospheric Science, Colorado State University, Fort Collins, Colorado, USA, [4] Department of Mathematics and Physical Science, University of Exeter, Exeter, UK, [5] Department of Environmental Science, Policy and Management, University of California, Berkeley, California, USA, [6] Institute of Agricultural Sciences, ETH Zurich, Zurich, Switzerland, [7] Department of Biology, University of New Mexico, Albuquerque, New Mexico, USA, [8] Department of Biological Sciences, Macquarie University, Sydney, New South Wales, Australia

Correspondence to: N. C. Parazoo, Nicholas.C.Parazoo@jpl.nasa.gov

Abstract

Climate extremes such as drought and heat waves can cause substantial reductions in terrestrial carbon uptake. Advancing projections of the carbon uptake response to future climate extremes depends on (1) identifying mechanistic links between the carbon cycle and atmospheric drivers, (2) detecting and attributing uptake changes, and (3) evaluating models of land response and atmospheric forcing. Here, we combine model simulations, remote sensing products, and ground observations to investigate the impact of climate variability on carbon uptake in the Texas-northern Mexico region. Specifically, we (1) examine the relationship between drought, carbon uptake, and variability of El Niño–Southern Oscillation (ENSO) and the North Atlantic Oscillation (NAO) using the Joint UK Land-Environment Simulator (JULES) biosphere simulations from 1950–2012, (2) quantify changes in carbon uptake during record drought conditions in 2011, and (3) evaluate JULES carbon uptake and soil moisture in 2011 using observations from remote sensing and a network of flux towers in the region. Long-term simulations reveal systematic decreases in regional-scale carbon uptake during negative phases of ENSO and NAO, including amplified reductions of gross primary production (GPP) ($-0.42 \pm 0.18\,\mathrm{Pg\,C\,yr^{-1}}$) and net ecosystem production (NEP) ($-0.14 \pm 0.11\,\mathrm{Pg\,C\,yr^{-1}}$) during strong La Niña years. The 2011 megadrought caused some of the largest declines of GPP ($-0.50\,\mathrm{Pg\,C\,yr^{-1}}$) and NEP ($-0.23\,\mathrm{Pg\,C\,yr^{-1}}$) in our simulations. In 2011, consistent declines were found in observations, including high correlation of GPP and surface soil moisture ($r = 0.82 \pm 0.23$, $p = 0.012$) in remote sensing-based products. These results suggest a large-scale response of carbon uptake to ENSO and NAO, and highlight a need to improve model predictions of ENSO

and NAO in order to improve predictions of future impacts on the carbon cycle and the associated feedbacks to climate change.

1 Introduction

Terrestrial ecosystem feedbacks to environmental changes result in global carbon sinks that are thought to mitigate greenhouse gas warming, but climate extremes such as drought and heat waves can cause substantial changes in regional carbon stocks that could release CO_2 to the atmosphere and potentially negate current and future sinks [*Reichstein et al*., 2013; *Schwalm et al*., 2012; *Zscheischler*, 2014a]. In North America, which represents a net sink of CO_2 in the present climate [*Xiao et al*., 2011; *King et al*., 2015], variations in carbon uptake are linked to changes in precipitation that affect ecosystem productivity [*Knapp et al*., 2002; *Xiao et al*., 2011; *Schwalm et al*., 2011]. In the western and Great Plains regions, declines in carbon sinks are observed during drought associated with drying and loss of productivity in croplands and grasslands [*Craine et al*., 2012; *Schwalm et al*., 2012; *Rajan et al*., 2013]. Droughts over the Great Plains, a key agricultural sector in the United States with a total market value of about $92 billion [*U.S. Department of Agriculture*, 2014], represent a threat to food security and energy production [*Smith and Katz*, 2013]. In the southern Great Plains region, which includes northern Mexico and Texas (denoted the TexMex domain, Figure 1, (106°W–93°W, 26°N–38°N), including Texas and surrounding grid cells), dramatic increases in the intensity and frequency of droughts are expected over the next century [*Seneviratne et al*., 2012; *Collins et al*., 2013]. Thus, projected drying will add stress to already limited water resources, affect management choices related to irrigation, municipal use, and energy generation [*Colby and Tanimoto*, 2011; *Shafer et al*., 2014], and potentially exacerbate climate-carbon feedbacks [*Collins et al*., 2013]. To obtain more reliable estimates of the sign and magnitude of future carbon cycle feedbacks and to improve drought preparedness in this critical agricultural region, improved quantification of the relationship between carbon uptake and drought in TexMex within the present climate is needed.

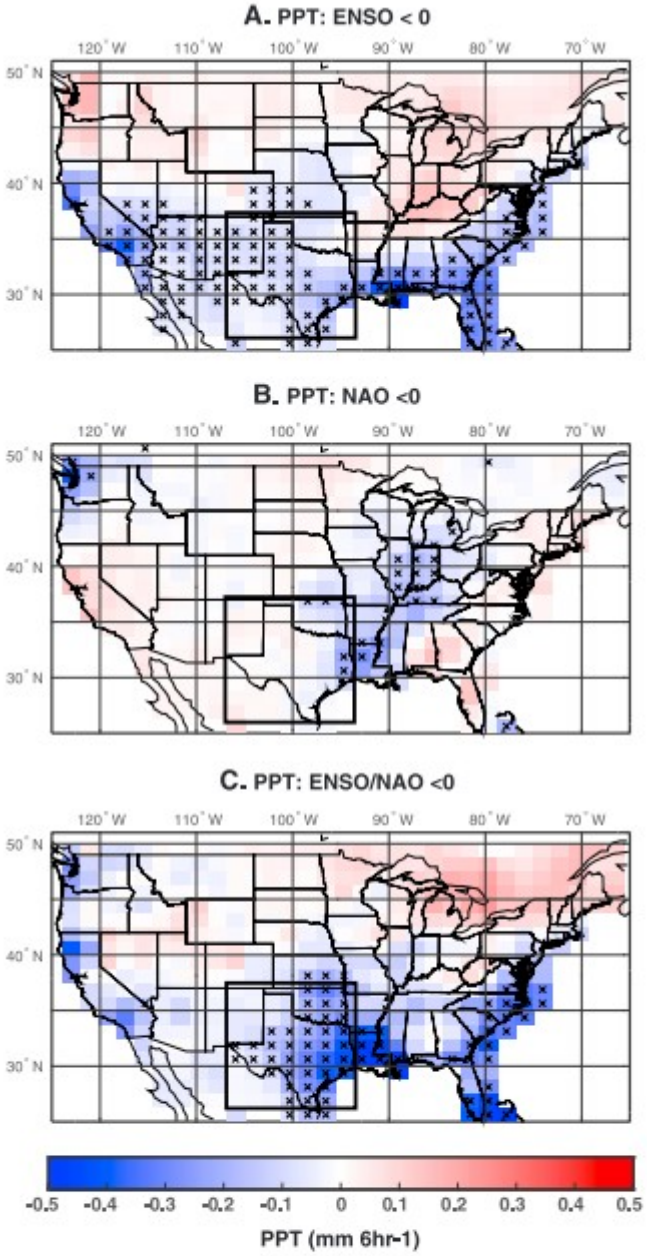

Figure 1. Maps of January–June averaged precipitation (PPT) anomalies for the period 1950–2012 for difference ENSO and NAO conditions, including (a) ENSO < 0, (b) NAO < 0, and (c) ENSO/NAO < 0. These conditions are classified using the ENSO and NAO winter average. Blue (red) shading represents negative (positive) anomaly. Stippling in Figure 1c represents points that exceed 2σ (standard deviation) based on bootstrapping methods (sample size = 5000). Rectangle denotes Texas-northern Mexico (TexMex) region of study.

Historically, climate models have failed to predict record droughts in TexMex [*Hoerling et al*., 2013; *Seager et al*., 2014]. It has been hypothesized that anomalies in atmospheric circulation patterns over the Great Plains related to ocean thermal forcing, atmospheric internal variability, and land-

atmosphere feedbacks play important and underrepresented roles [*Seager et al*., 2014]. The most commonly accepted cause of drought in TexMex has been cold tropical Pacific sea surface temperature (SST) anomalies associated with La Niña patterns, which can coalesce with other SST anomalies in the Atlantic and Indian Oceans and lead to extreme droughts [*Nigam et al*., 2011, and references therein]. La Niñas are characterized by anticyclonic high anomalies in the North Pacific that merge with a zonal band of high pressure across North America into the mid-Atlantic Ocean [*Seager et al*., 2014]. This typically leads to dry conditions in southern parts of North America, especially along the Gulf Coast, with peak drying in winter, weak drying in spring, and a return to normal conditions in summer.

However, La Niñas do not necessarily lead to summer droughts, and some severe to extreme droughts occurred without clear forcing from SST anomalies [e.g., *Namias*, 1991]. These droughts have been often attributed to atmospheric internal variability including negative winter phases of the North Atlantic Oscillation (NAO) [*Hoerling et al*., 2013; *Seager et al*., 2014], which help initiate or intensify droughts, and land surface feedbacks [e.g., *Myoung and Nielsen-Gammon*, 2010, and references therein], which can sustain droughts. The NAO is characterized by positive geopotential height anomalies over the Icelandic region and below normal heights in the western Atlantic and across eastern and southern North America [*Hurrell and Deser*, 2009]. The resulting decreased pressure gradient reduces the westerlies and causes high-latitude blocking of storm tracks, which drives advection of cold and dry air from Alaska and Canada into the United States and can lead to negative precipitation anomalies in TexMex. Through land-atmosphere feedbacks, low soil moisture availability and evapotranspiration (ET) can feed back onto the atmospheric processes controlling clouds, rainfall, and radiation, which can reinforce drying [*Seneviratne et al*., 2010]. Reduced stomatal conductance through increased vapor pressure deficit can lead to additional reductions of ET rates across the land surface [*Sellers et al*., 1997]. Modeling the impact of these processes on drought persistence relies fundamentally on the ability to represent soil moisture-vegetation interactions.

In 2011, TexMex experienced one of the worst droughts on record (denoted as TMD11), with severe drought conditions lasting from winter 2010-2011 through fall 2011 and with record low precipitation (40% of average) during the 2011 water year [*Long et al*., 2013]. Although short relative to the record-setting multiyear droughts of the 1930s and 1950s, TMD11 was the worst drought period in the region since the mid-1950s [*LeComte*, 2012]. Abnormally dry conditions persisted from winter through summer, with record warm summer temperatures throughout TexMex [*Hoerling et al*., 2013; *Seager et al*., 2014].

The abnormally dry conditions during peak rainy months in late winter/early spring cut off a critical supply of soil moisture for plants and agriculture during the summer growing season [*Long et al*., 2013], leading to $7.6 billion

in agricultural losses [*Fannin*, 2012] and conversion of a pasture site in northern Texas from a CO_2 sink in 2012 to a source in 2013 driven by declines in gross primary production (GPP) [*Rajan et al*., 2013]. Semiempirical evidence suggests that drought-induced GPP loss was widespread and significant, likely impacting the entire TexMex region and representing one of the largest negative spatiotemporal GPP anomalies over the last 30 years in North America [*Zscheischler et al*., 2014a].

During typical TexMex droughts the primary forcing mechanisms of La Niña, internal atmospheric variability, and land surface feedbacks work separately. TMD11, however, was likely driven by a combination of all three, with drought onset in winter and spring forced initially by La Niña, and then sustained and likely exacerbated into summer by atmospheric moisture divergence across the TexMex region related to the negative phase of the NAO in winter 2010-2011 and land surface feedbacks [*Hoerling et al*., 2013; *Seager et al*., 2014]. TMD11 was well represented in models constrained by observed SST anomalies and atmospheric observational reanalysis but poorly represented in coupled climate models [*Hoerling et al*., 2013].

These studies imply a regional-scale (~1000 km's) sensitivity of semiarid ecosystem productivity across the TexMex region to drought-induced water stress associated with atmospheric circulation anomalies during negative phases of El Niño–Southern Oscillation (ENSO) and the NAO. This link has been observed at small scales in the case of TMD11, but it is unclear whether there is a systematic regional-scale response of net carbon uptake in TexMex to variations of ENSO and the NAO.

Here we examine the regional-scale carbon uptake response of TexMex region to La Niña and negative NAO events from 1950 to 2012. We first examine the relationship between drought, carbon uptake, and variability of ENSO and the NAO using simulations of the Joint UK Land-Environment Simulator (JULES) terrestrial biosphere model from 1950 to 2012. This will help determine the sensitivity of TexMex carbon uptake to variations of La Niña and the NAO and provide a climatological context to evaluate the significance of the extreme 2011 drought event. Due to limitations in the predictability of ENSO and the NAO in free-running climate models, JULES simulations are forced by observed climate to ensure proper atmospheric forcing and attribution of carbon uptake drivers. We then compare JULES predictions of carbon uptake and soil moisture to observations from flux towers and satellites during TMD11. Thus, TMD11 serves as a case study to evaluate JULES and to determine the predictability of the impact of meteorological drought on modeled soil moisture and carbon uptake.

We ask four main questions: (1) Are large-scale changes in TexMex carbon uptake linked fundamentally to water deficits associated with negative phases of ENSO and the NAO? And (2) are these relationships robust over the climatological record? (3) Are carbon uptake changes during TMD11 present and detectable with remote sensing techniques and consistent with in situ

measurements from flux towers? (4) How well does JULES predict this impact?

2 Methods

2.1 Approach

We first examine the relationship between La Niña, the NAO, drought, and carbon uptake using JULES simulations from 1950 to 2012, which provides a long time scale over which we seek to capture a large sample size of climate events and establish potentially statistically meaningful relationships. JULES predictions of soil moisture and carbon uptake anomalies during TMD11 are then evaluated against a suite of satellite and flux tower observations. Soil moisture anomalies are compared to measurements of total column and surface soil moisture from the Gravity Recovery and Climate Experiment (GRACE) and Soil Moisture and Ocean Salinity (SMOS) satellites, respectively. GPP and net ecosystem production (NEP) are evaluated at local scale against eddy covariance flux tower sites. GPP is also evaluated regionally using observations of canopy photosynthesis derived from satellite retrievals of solar-induced chlorophyll fluorescence (SIF) from the Greenhouse gases Observing SATellite (GOSAT). All model and observation time series are based on the average of pixels within the TexMex domain (106°W–93°W, 26°N–38°N).

2.2 Observations

2.2.1 Regional Carbon Uptake

Simulations of regional GPP anomalies are evaluated against three remote sensing-based GPP estimates. The first, denoted GOPT, is derived from an ensemble of terrestrial biosphere models constrained by GOSAT SIF measurements. The second, denoted MOD17 (Moderate Resolution Imaging Spectroradiometer (MODIS) MOD17A2 GPP product), is derived from a light use efficiency model constrained by MODIS canopy greenness observations. The third, denoted as Max Planck Institute (MPI), is derived from a flux tower data based upscaling approach using the Max Planck Institute for Biogeochemistry (MPI-BGC) model. These three semiempirical GPP estimates are described in order below.

SIF is visible solar energy reemitted at longer wavelengths from the chlorophyll of assimilating leaves, and thus originates from the core complexes of the photosynthetic machinery. Global measurements of SIF have opened up the possibility to estimate the rate of planetary photosynthesis at increasing spatial resolution (down to ~10.5 km diameter in GOSAT), providing direct seasonal constraints on global GPP [*Frankenberg et al.*, 2011]. Near global retrievals of SIF from GOSAT correlate strongly ($r^2 = 0.80$) at global annual scale with flux measurement-based GPP extrapolated globally from the MPI approach [*Frankenberg et al.*, 2011; *Beer et al.*, 2010; *Jung et al.*, 2011]. There are two key advantages for using SIF in the present study.

1. SIF is directly proportional to absorbed photosynthetically active radiation seen by chlorophyll, rather than the nonphotosynthesizing parts of the plant and/or soil/surfaces. Spaceborne SIF measurements are, therefore, sensitive only to variations in the rate of photosynthesis rather than changes in reflectance not associated with vegetation. This is an important benefit in sparsely vegetated semiarid regions such as TexMex.
2. SIF can be used to estimate actual photosynthesis rather than potential photosynthesis and can detect plant physiological effects and plant productivity changes linked to water limitation and temperature stress [*Daumard et al*., 2010; *Lee et al*., 2013]. SIF remote sensing data, therefore, offers crucial insight into regional impacts of drought events such as TMD11.

For GOPT, we use a Bayesian analysis framework to estimate monthly averaged GPP at 5° × 4° grid spacing that optimally accounts for uncertainties in predictions of GPP from terrestrial biosphere models, estimates of GPP inferred from satellite observations of midday SIF, and relationships between SIF and GPP [*Parazoo et al*., 2014]. Here prior GPP is predicted from 1950 to 2012 using JULES (see below). Uncertainty is estimated using the spread of eight biosphere models from the TRENDY model intercomparison project over the period 2000–2009 (http://dgvm.ceh.ac.uk/node/9) [*Sitch et al*., 2015]. Midday SIF is taken from GOSAT from 2009 to 2012 and scaled to monthly GPP using the empirical linear relationship with MPI GPP with careful accounting for uncertainties in SIF measurements and the MPI approach [*Frankenberg et al*., 2011; *Parazoo et al*., 2014].

We note that while this method provides an uncertainty range based on model climatology, the limited period of available model data means we are unable to account for possible changes in uncertainty during the 2011 drought. However, this methodology does provide estimates of posterior uncertainty based on assimilation of year specific satellite SIF data, leading to significant uncertainty reductions (exceeding 50% in many cases) in regions where observational coverage and prior uncertainty are high. The combination of GOPT and uncertainty in this study provides a regional semiempirical GPP constraint, helps to quantify the significance of regional GPP changes, and provides a range of uncertainty for determining the significance of predicted GPP.

Although GOPT is constrained by critical satellite SIF measurements, it relies fundamentally on GPP output from terrestrial biosphere models, which in this study is JULES. Consequently, GOPT cannot be used as an independent model evaluation product for regional GPP. For this, we rely on data sets from the MODIS MOD17A2 GPP product (MOD17) [*Running et al*., 2004; *Myneni et al*., 2007] and from the Biogeochemical Model-Data Integration Group of the Max Planck Institute for Biogeochemistry (MPI) [*Beer et al*.,

2010; *Jung et al*., 2011]. Both the MOD17 and MPI GPP data sets rely on satellite-derived estimates of the fraction of absorbed photosynthetically active radiation (FAPAR) to model GPP. MODIS GPP is based on the combination of tabulated light use efficiency with meteorological parameters and FAPAR, whereas MPI GPP is produced by the global upscaling of flux tower measurements of CO_2, water, and energy fluxes.

2.2.2 Regional Soil Moisture

Changes in soil water from 2009 to 2012 are derived from GRACE [*Swenson and Wahr*, 2006; *Landerer and Swenson*, 2012] and SMOS. GRACE, which consists of two satellites that monitor distances between each other to track temporal variation in Earth's gravity field [*Tapley et al*., 2004], provides global estimates of satellite-derived changes in liquid water equivalent (LWE) thickness (units of cm's) and therefore acts as a remote sensing drought indicator [e.g., *Long et al*., 2013]. We use 2009–2012 LWE from Release 05 GRACE-Tellus, which is provided at monthly resolution on a global 1° × 1° grid (data access from http://catds.ifremer.fr/Products/Products-access).

SMOS is a passive microwave interferometer, using the band at 1.4 GHz [*Kerr et al*., 2010]. It provides surface soil moisture (top 5 cm) at 6 A.M. and 6 P.M. and covers the entire Earth surface within 3 days. The satellite was launched in November 2009, and data are available since 2010. SMOS soil moisture from 2010 to 2011 is taken from the reprocessed Version 1 Level 3 Centre Aval de Traitement des Données (CATDS) aggregated monthly product on a 25 km × 25 km equal area scalable Earth grid, using the average of ascending and descending orbits [*Jacquette et al*., 2010] (data access from www.catds.fr/sipad).

2.2.3 Flux Tower Measurements

We used direct measurements of half-hourly net ecosystem productivity (NEP) from five eddy covariance flux tower sites in New Mexico (New Mexico Elevation Gradient) and Texas (Table 1) to quantify the biosphere-atmosphere CO_2 exchange. GPP was estimated from measured nighttime NEP (total ecosystem respiration, TER) with extrapolated temperature response functions. These data were collected and processed as described in *Anderson-Teixera et al*. [2011], gap-filled using meteorological data, and aggregated to monthly sums of CO_2 exchange.

Table 1. Site Characteristics of Eddy Covariance Flux Towers[a]

Site Name	Site ID	IGBP	Latitude	Longitude	Elevation	Site Years
Freeman Ranch Mesquite Juniper	US-FR2	WSA	29.9495	−97.9962	272	2005–2012
HLC Pinyon Juniper Woodland	US-Mpj	OSH	34.4384	−106.2377	2138	2008–2012
Tablelands Juniper Savanna	US-Wjs	OSH	34.4255	−105.8615	1926	2008–2012
Valles Caldera Mixed Conifer	US-Vcm	ENF	35.8884	−106.5321	3003	2007–2012
Valles Caldera Ponderosa Pine	US-Vcp	ENF	35.8624	−106.5974	2542	2007–2012

[a]The IGBP land use classes correspond to woody savanna, open shrubland (OSH), and evergreen needleleaf forest (ENF). Elevation is denoted as meter asl.

2.3 Biosphere Model Simulations

JULES (the Joint UK Land-Environment Simulator) is the land surface model of the Hadley Centre climate model [*Cox et al*., 2000; *Cox*, 2001; *Essery et al*., 2003]. It simulates fluxes of carbon, water, and energy on nine tiles, including five plant functional types (broadleaf tree, needleleaf tree, C3 and C4 grasses, and shrub). The biophysics is based on *Collatz et al*. [1991, 1992] for C3 and C4 photosynthesis. Potential (nonwater stressed) photosynthesis is calculated as a smoothed minimum of three rates: rubisco limited, light limited, and either rate of transport of photosynthetic products (for C3) or phosphoenolpyruvic acid carboxylase limitation (for C4). The JULES canopy has 10 layers, with the leaf area index for each being divided into sunlit and shaded fractions. A two-stream approximation of radiation interception [*Sellers*, 1985] is used to calculate spectral albedos and absorbed incoming radiation for each layer, allowing for penetration of direct-beam sunflecks into the canopy. A soil moisture stress factor directly reduces the potential photosynthesis rate. Leaf-level net photosynthesis is related to stomatal conductance based on a CO_2 diffusion equation and the leaf humidity deficit [*Jacobs*, 1994; *Cox et al*., 1998]. Within JULES, Top-down Representation of Interactive Foliage and Flora Including Dynamics (TRIFFID) predicts fractional coverage of each plant functional type (PFT), soil carbon, vegetation carbon, and leaf area index. For each PFT, the change in fractional coverage is based on the net carbon available to it and a Lotka-Volterra competition scheme [*Cox*, 2001]. Soil carbon is modeled in four pools, and respiration is based on the RothC model. Full model details are available in *Clark et al*. [2011] and *Best et al*. [2011].

JULES is forced over the period 1860–2013 at 1.875° × 1.25° using a factorial set of sensitivity simulations. Here we use monthly mean GPP output from "S3" simulations forced with changing CO_2, land use change, and climate information from the Climatic Research Unit-National Centers for Environmental Prediction (CRU-NCEP) data set, representing the combination of CRU TS.3.2 0.5° × 0.5° monthly climatology and NCEP reanalysis 2.5° × 2.5° 6-hourly data (ftp://nacp.ornl.gov/synthesis/2009/frescati/model_driver/cru_ncep/analysis/readme.htm).

We are interested in anomalies of climate and ecosystem function during a subset of negative ENSO and NAO years relative to 1950–2012 climatology. To calculate anomalies over this period, data are deseasonalized (mean seasonal average removed), averaged temporally over the period of interest, and then detrended using a forward and reverse low-pass frequency filter of order 5 and cutoff frequency 0.15. After deseasonalizing and detrending, variables are either averaged over growing season months of April to September to reflect the peak period of photosynthetic activity or January to June to reflect the period of peak precipitation deficits in La Niña years.

We test for significance of anomalies using a bootstrap approach [e.g., *Efron*, 1979] in which we create a sample of 5000 random samples each of length M subsampled from the simulated time series of length N. For this study, $N = 63$, representing the number of years from 1950 to 2012, and M varies for different composite subsamples. We then test for 90% significance by searching for composite averages that either fall above the highest 10 percentile level (for positive anomalies) or below the lowest 10 percentile level (for negative anomalies) of the bootstrap average and denote significance graphically with symbol (circles for time series and crosses for maps). We note that significance estimates were recalculated using 1000 random samples with nearly identical results, suggesting that our choice of 5000 samples is considered large enough for significance testing.

2.4 Semiarid Ecosystems in TexMex

We quantify semiarid and individual PFT contribution to TexMex carbon budgets during the 2011 drought using PFT classifications from (1) JULES and (2) the International Geosphere-Biosphere Programme (IGBP). JULES consists of five main vegetation PFTs including needleleaf forests (1%), broadleaf forests (2%), C3 grass (25%), C4 grass (33%), shrublands (2%), and other nonvegetated tiles including 36% bare soil. Croplands are not included in this model version. For IGBP, we use a modified classification following *Frankenberg et al*. [2011] consisting of needleleaf (<1%), evergreen broadleaf (<1%), deciduous broadleaf (5%), shrubland (31%), savannah (9%), grassland (38%), cropland (11%), and other nonvegetated tiles (5%). Based on these classifications, we estimate that semiarid ecosystems (shrublands, savannah, grassland, cropland, and bare soil) represent 96% and 89% of TexMex vegetation, respectively. PFT contributions to GPP loss in semiempirical (GOPT) and model (JULES) estimates are discussed in section 3.4.

2.5 Climate Indices for La Niña and the NAO

ENSO conditions are defined based on SST variations and their persistence along the equatorial Pacific Ocean and determined from the Oceanic Niña Index (ONI), which is based on a 3 month running mean of SST anomalies in the Niño-3.4 region (5°S–5°N, 120°W–170°W) calculated by the National Oceanic and Space Administration (NOAA) climate prediction center (CPC) (http://www.cpc.ncep.noaa.gov/products/analysis_monitoring/ensostuff/

ensoyears.shtml) [*L'Heureux et al*., 2012]. NOAA defines El Niño and La Niña episodes based on a monthly ONI threshold of ± 0.5°C; in this study, we define these episodes based on a winter average (December-January-February, or DJF) ONI threshold of ± 0.0°C. We refer to DJF ONI averages as ENSO and El Niño/La Niña episodes as ENSO > 0 and ENSO < 0, respectively. ENSO episodes over the period 1950–2012 are shown in Figure 2a.

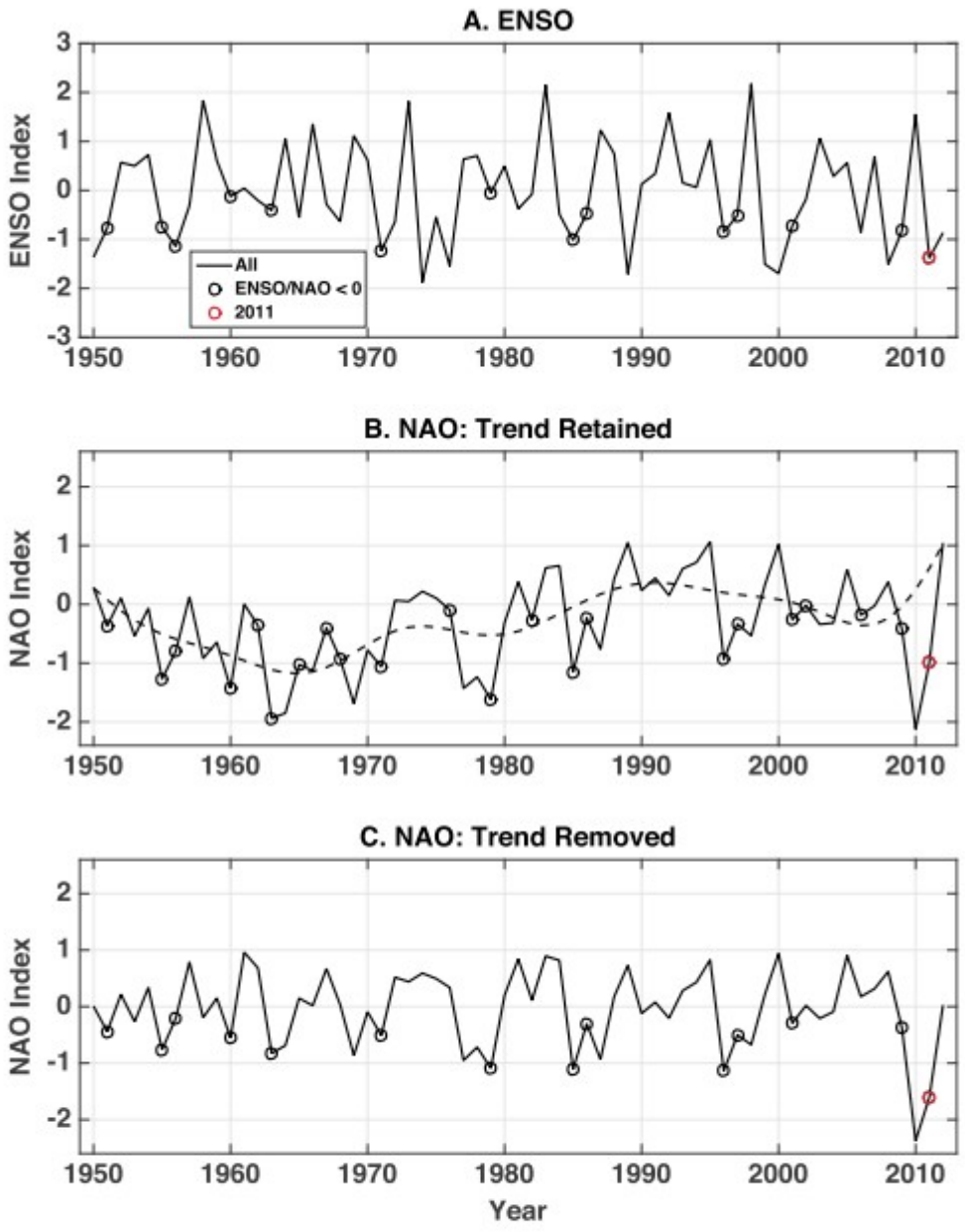

Figure 2. Time series of winter (DJF) climate modes from 1950 to 2012, including (a) detrended ENSO, (b) NAO, and (c) detrended NAO. Years when detrended ENSO < 0 and detrended NAO < 0 are represented by black circles in Figures 2a and 2c. Circles in Figure 2b represent years with trended NAO < 0. Red circles are 2011.

The NAO index consists of a north-south dipole of surface pressure anomalies, with one centered over Greenland and the other of opposite sign spanning the North Atlantic from 35°N to 40°N [*Barnston and Livezey*, 1987]. Here we use the monthly tabulated NAO index from 1950 to 2012 calculated by the CPC and based on monthly standardized 500 mb height anomalies

obtained from the NCEP/National Center for Atmospheric Research reanalysis data set (http://www.cpc.ncep.noaa.gov/products/precip/CWlink/pna/nao.shtml). The NAO, unlike ENSO, is normalized using the 1981–2010 base period. Consequently, the NAO DJF average shows significant decadal trends resembling a sinusoid (Figure 2b), with low values in the 1960s and high values in the late 1980s/early 1990s. To examine the sensitivity of interannual variability in ecosystem function to interannual variability in winter NAO, we remove the decadal harmonic using a high-pass filter. Detrended values are shown in Figure 2c and will be used for the remainder of this study. However, we repeat this analysis with the decadal trend retained to investigate sensitivity of carbon uptake and ET to persistent decadal NAO effects.

Note that the ENSO/NAO indices are the CPC values rather than the indices computed using the CRU-NCEP fields; however, this is not expected to influence the conclusions of this study since CRU-NCEP fields are based on assimilated meteorological observations. Unless stated otherwise, all results are based on negative index winters (ENSO < 0 and NAO < 0) and denoted throughout the paper as ENSO/NAO < 0 years. ENSO/NAO < 0 years, circled in Figures 2a and 2c, occur 22% of the time, or 14 out of 63 years (see Table 2), with at least two events per decade over the 63 year record.

Table 2. Anomalies of Enviroclimatic and Ecosystem Function Variables for Different ENSO and NAO Cases, Selected According to Deviation From Zero (Row 1)[a]

Filtering Criteria	ENSO < 0 NAO < 0	ENSO < 0 NAO $< -1\sigma$	ENSO $< -1\sigma$ NAO < 0	ENSO $< -1\sigma$ NAO < 0 (Excluding 2011)	ENSO $< -1\sigma$ NAO $< -1\sigma$
Years retained (out of 63)	14	6	3	2	1
PPT Feb–Jul (mm 6 h^{-1})	-0.095 ± 0.32	-0.13 ± 0.38	-0.48 ± 0.14	-0.41 ± 0.092	-0.62
GPP Jan–Dec (Pg C yr^{-1})	-0.069 ± 0.29	-0.16 ± 0.29	-0.42 ± 0.18	-0.37 ± 0.23	-0.50
TER Jan–Dec (Pg C yr^{-1})	-0.053 ± 0.20	-0.11 ± 0.17	-0.28 ± 0.080	-0.28 ± 0.11	-0.27
NEP Jan–Dec (Pg C yr^{-1})	-0.017 ± 0.11	-0.047 ± 0.14	-0.14 ± 0.11	-0.09 ± 0.12	-0.23
ET Apr–Sep (kg m^{-2} s^{-1})	-0.055 ± 0.30	-0.077 ± 0.35	-0.46 ± 0.23	-0.37 ± 0.25	-0.64
SoilW Apr–Sep (kg m^{-2})	-6.2 ± 21.6	-10.6 ± 23.1	-30.7 ± 7.2	-33.32 ± 7.9	-25.5
SWdwn Feb–Jul (W m^{-2})	1.16 ± 2.17	1.11 ± 2.89	4.14 ± 1.18	3.46 ± 0.04	5.5
Ts Apr–Sep (K)	0.15 ± 0.66	0.25 ± 0.79	0.67 ± 0.46	0.50 ± 0.51	1.0
LAI Apr–Sep (m^2 m^{-2})	-0.02 ± 0.09	-0.023 ± 0.09	-0.12 ± 0.03	-0.14 ± 0.03	-0.085

[a]Statistics include number of years for each case (row 2) and average ± standard deviation of anomalies (rows 3–8). Column 1 shows variable of interest, averaging period, and units. Most fields are averaged during the growing season (Apr–Sep) except PPT and SWdwn (Feb–Jul) and GPP and NEP (Jan–Dec). Carbon fluxes (GPP, TER, and NEP) are annual sums.

3 Results and Discussion

3.1 Changes in Carbon Uptake During Negative Phases of ENSO and the NAO

Analysis of CRU-NCEP meteorology from January to June over the period 1950–2012 show strong negative precipitation (PPT) anomalies during La Niña years (ENSO < 0) throughout the southern portion of North America, including TexMex, the Midwest, and most strongly along the Gulf Coast (Figure 1a), with most grid points exceeding 90% significance (estimated from a bootstrap test and indicated by crosses). Negative anomalies also occur in NAO < 0 years (Figure 1b) but are more regional, limited primarily to eastern Texas and extending north-northeast to the Great Lakes region. However, negative anomalies are strongly amplified in TexMex during

overlapping negative phases of ENSO and the NAO (ENSO/NAO < 0 years, Figure 1c), leading to a 10% deviation from climatology in winter and spring when PPT is near its annual minimum (Figure 3a). While negative anomalies of monthly area integrated PPT are generally not significant during this period (with the exception of December and March as indicated by circles in Figure 3), grid-scale time integrated values exceed 90% significance throughout TexMex in ENSO/NAO < 0 years (crosses in Figure 1c). These results suggest that La Niña drives precipitation decreases throughout southern North America, including TexMex, with amplification of precipitation decreases in TexMex during concurrent phases of negative winter NAO.

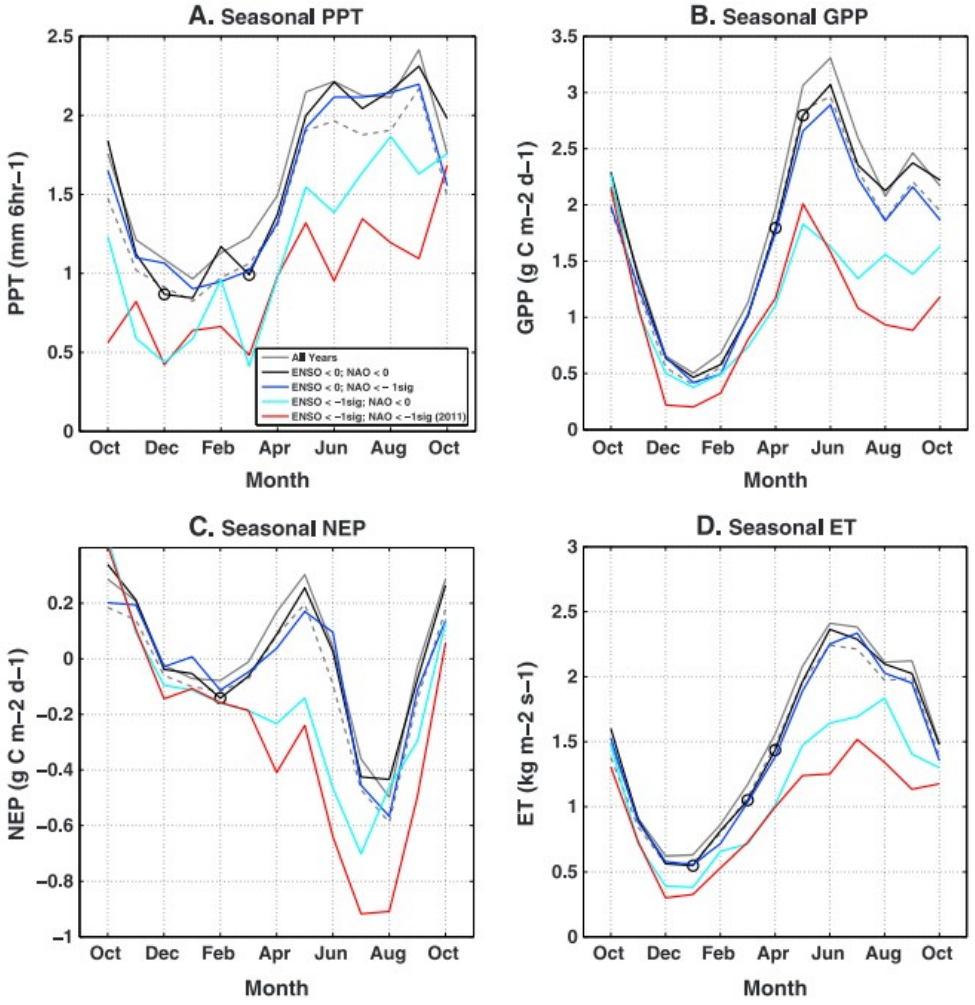

Figure 3. Seasonal averages of (a) precipitation (PPT), (b) gross primary production (GPP), (c) net ecosystem production (NEP, positive represents carbon uptake from atmosphere), and (d) evapotranspiration (ET) averaged across the TexMex water year (October–September) for a range of ENSO and NAO conditions from 1950 to 2012. Averages include all years (grey), years with ENSO < 0 and NAO < 0 (black), years with ENSO < 0 and NAO $< -1\sigma$ (blue), years with ENSO $< -1\sigma$ and NAO < 0 (cyan), and years with ENSO $< -1\sigma$ and NAO $< -1\sigma$ (red). GPP, NEP, and ET are computed from JULES. Grey dashed line represents the lower 90% significance threshold, estimated from bootstrapping methods (sample size = 5000). Circles represent months that exceed 90% significance during years in which ENSO < 0 and NAO < 0.

Model results show corresponding declines of carbon flux (GPP and NEP) and ET in winter, spring, and summer in ENSO/NAO < 0 years (Figures 3b–3d). Negative GPP anomalies exceed 90% significance at the beginning of the growing season (April and May) and are the primary driver of reduced carbon uptake by NEP (Figure 3c), which is subject to the strongest declines during winter (stronger source) and spring (weaker sink). Negative anomalies of TER, representing ~75% of GPP, reduce the overall magnitude of NEP anomalies. This simultaneous decrease in GPP and TER during drought including stronger GPP reductions is consistent with model and observational studies [*Law et al*., 2001; *Schwalm et al*., 2010; *Zscheischler et al*., 2014b]. ET is composed primarily of soil evaporation in this region (~80% of total ET); and hence, negative anomalies of ET are driven mainly by reductions in evaporation rather than plant transpiration. GPP, NEP, and ET reductions in ENSO/NAO < 0 years are generally much weaker toward the end of the growing season as precipitation returns to normal.

Anomalies of spring PPT and growing season carbon flux and ET are weakly (correlation ranges from 0.16 to 0.22), but positively, correlated with ENSO (grey points in Figure 4) with net negative anomalies during ENSO < 0 years and positive anomalies for ENSO > 0 years. However, high standard error and weak slope of regression indicate that ENSO by itself does not explain a significant amount of PPT and carbon flux variability in TexMex. These relationships are much stronger during ENSO/NAO < 0 years (black points in Figure 4), including a factor of 8–10 higher regression slopes and a factor of 3–4 higher correlation (correlation ranges from 0.53 to 0.64), and thus the amount of variance explained by ENSO is much higher when indices for ENSO and the NAO are both negative.

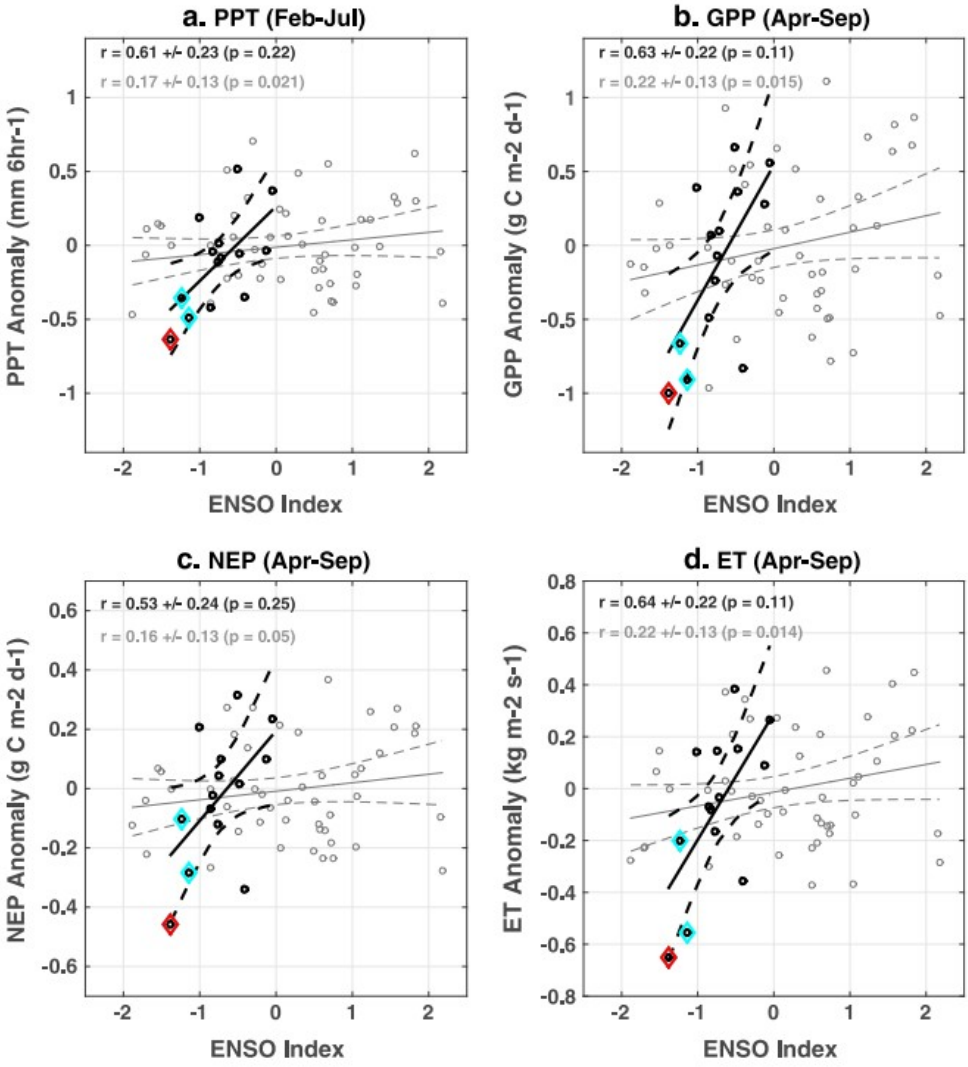

Figure 4. Scatterplots of monthly anomalies of JULES model predictions against ENSO, including (a) precipitation (PPT), (b) gross primary production (GPP), (c) net ecosystem production (NEP), and (d) evapotranspiration (ET) against ENSO. Grey represents all years and black years where ENSO/NAO < 0. Red diamonds represent years with ENSO $< -1\sigma$ and NAO $< -1\sigma$. Cyan diamonds are years with ENSO $< -1\sigma$ and NAO < 0 (includes red diamond). Solid lines are linear regressions, and dashed the 95% confidence bounds. Correlation (r) and p value (p) are color coded for each regression.

Similar results are obtained for ENSO/NAO < 0 years when repeating the analysis with decadal NAO trends retained (not shown) including the positive correlation of GPP and ET with ENSO ($r = 0.43 \pm 0.20$ ($p = 0.11$) and 0.38 ± 0.21 ($p = 0.11$), respectively). The model relationships are degraded, however, suggesting that year-to-year variability in climate plays a strong role in ecosystem function in TexMex during this period. More broadly, these results strongly support a mechanistic link between atmospheric circulation patterns and regional carbon cycles across TexMex during overlapping negative phases of ENSO (La Niña) and the NAO in which spring precipitation deficits are correlated with reductions of growing season carbon uptake and ET.

3.2 Drivers of Reduced Carbon Uptake During Concurrent Negative Phases of ENSO and the NAO

Perturbations to ecosystem function are forced by a combination of environmental impacts and changes to plant structure. For example, field experiments at a semiarid pasture site in Texas provide evidence of an immediate physiological response of GPP to soil moisture stress in 2011 related to stomatal closure and reduced photosynthesis [*Rajan et al.*, 2013]. Texas incurred $7.6 billion in agricultural losses [*Fannin*, 2012], suggesting large-scale decline in biomass in 2011, which is related to losses in GPP and NEP. We investigate climate (soil moisture and temperature) and plant structure (leaf area index) effects in JULES using correlation statistics.

JULES shows a weak positive relationship of ENSO with total soil moisture anomalies (SoilW, $r = 0.35 \pm 0.12$, $p = 0.036$) and weak negative relationships with downward shortwave radiation (SWdwn, $r = -0.35 \pm 0.12$, $p = 0.012$), and air temperature (Ts, $r = -0.12 \pm 0.13$, $p = 0.054$) over the period 1950–2012. These sensitivities are strongly enhanced, however, during ENSO/NAO < 0 years (SoilW: $r = 0.56 \pm 0.24$, $p = 0.01$; SWdwn: $r = -0.65 \pm 0.22$, $p = 0.0036$; Ts: $r = -0.52 \pm 0.25$, $p = 0.51$). Moreover, anomalies of SoilW and GPP are well correlated ($r = 0.94 \pm 0.10$, $p = 0.0038$), consistent with observational evidence in this and previous studies. Negative soil moisture anomalies also explain our findings of reduced ET driven by soil evaporation.

We note that negative precipitation anomalies peak from November through May, while GPP anomalies peak later into the growing season (Figure 4a). Enhanced correlation of PPT with GPP and SoilW at a time lag of 2 months ($r = 0.93 \pm 0.11$ ($p = 0.000001$) and 0.83 ± 0.16 ($p = 0.0002$), respectively) compared to zero time lag ($r = 0.65 \pm 0.22$ ($p = 0.014$) and 0.45 ± 0.26 ($p = 0.11$)) indicates a delayed response of soil moisture and plant physiology to precipitation deficits, suggesting that winter and spring precipitation anomalies produce carbon cycle feedbacks well into summer (hence, the choice of the February to July averaging period for PPT in Figure 4a and Table 2).

JULES shows a significant positive correlation of leaf area index (LAI) with ENSO in ENSO/NAO < 0 years ($r = 0.72 \pm 0.20$, $p = 0.12$) and strong sensitivity of LAI to ENSO intensity (slope $= 0.19\ \mathrm{m^2\ m^{-2}}$/ENSO index, factor of 10 stronger than slope of all years combined). Despite high correlation of JULES LAI and ENSO, total LAI loss in ENSO/NAO < 0 years is small compared to average LAI in this region (<5%) and is therefore unlikely to have a significant impact on simulated GPP.

Typically, JULES GPP is very closely balanced by TER in TexMex such that annual NEP is close to zero ($-0.004\ \mathrm{Pg\ C\ yr^{-1}}$) and TexMex is carbon neutral. However, we have shown that JULES GPP anomalies ($-0.069 \pm 0.29\ \mathrm{Pg\ C\ yr^{-1}}$) exceed TER anomalies ($-0.053 \pm 0.20\ \mathrm{Pg\ C\ yr^{-1}}$) during ENSO/NAO < 0 years leading to reduced NEP and converting the region into a slightly stronger (though still insignificant) carbon source ($-0.017 \pm 0.20\ \mathrm{Pg\ C\ yr^{-1}}$). TER is

driven by a combination of autotrophic respiration (R_A) during plant growth and maintenance and heterotrophic respiration (R_H) by microbial decomposition of soil carbon. In JULES, both terms are sensitive primarily to changes in soil moisture and soil temperature, with high R_H sensitivity to soil moisture in dry soils well reproducing observed responses [*Clark et al.*, 2011]. Low soil moisture in Texas in 2011 caused a decrease in R_A nearly proportional to GPP (through photosynthesis), but water limitation effects on R_H were partly balanced by high soil temperature, driving an increase in R_H and net decrease of NEP [*Rajan et al.*, 2013]. However, during typical ENSO/NAO < 0 years, JULES shows negative anomalies of both terms, with 65% of the anomaly driven by R_A ($-0.034\,\mathrm{Pg\,C\,yr^{-1}}$) and 35% by R_H ($-0.018\,\mathrm{Pg\,C\,yr^{-1}}$). Given the very small change in JULES Ts during these years ($+0.15\,\mathrm{K}$), it is likely that soil moisture deficits drive decreased R_A and R_H during ENSO/NAO < 0 years and heat stress effects are small.

The above analysis suggests that decreases in carbon uptake and ET are driven by a combination of environmental stress and degradation of plant biomass, and that these responses are amplified with increasing La Niña strength during ENSO/NAO < 0 years. There is, however, significant variability across the 14 identified events (see Figure 2), which precludes a potential systematic environmental and ecosystem response to spring precipitation deficits during these periods. For example, if we classify a “negative response” as enhanced environmental stress (negative anomalies of PPT and SoilW and positive anomalies of SWdwn and Ts) and reduced ecosystem function (negative anomalies of carbon uptake, ET, and LAI) and a “positive response” as the reverse, we find in general a negative response during strong La Niña years and a positive response during weak La Niña years (Figure 4). The average of anomalies and corresponding variability for each of these fields during ENSO/NAO < 0 is shown numerically in Table 2 (column 2). In all cases, variability exceeds the anomaly; and hence, these anomalies are not considered significant. The implication is that changes in ecosystem function are not predictable given only information about the sign of ENSO and NAO phases. In order to identify a potentially systematic ecosystem response to atmospheric circulation anomalies associated with internal atmospheric variability, further filtering of ENSO and NAO conditions is needed.

3.3 Enhanced Carbon Uptake Reduction With Increasing Intensity of ENSO and the NAO

We investigate these relationships further by sorting ENSO/NAO < 0 years based on ENSO and the NAO strength, since these events can affect precipitation in TexMex independent of each other (see Figure 2). We classify these new conditions using 1σ deviations of ENSO and NAO from zero. Sorting by negative ENSO years (ENSO < 0) and strongly negative NAO years (NAO $< -1\sigma$, $\sigma = 0.68$) reduces the total number of events from 14 to 6 (1955, 1963, 1979, 1985, 1996, and 2011; Table 2, column 3). This increases the magnitude of annual anomalies for each environmental and ecosystem

anomaly, with the strongest effects on PPT, carbon uptake, and SoilW in late spring and summer (Figure 3, blue), but these anomalies are still exceeded by year-to-year variability. Increasing severity of NAO alone does not lead to systematic changes in carbon uptake across TexMex.

Sorting based on strong La Niña years (ENSO $< -1\sigma$, $\sigma = 1.02$) and negative NAO years (NAO < 0) further reduces the number of events from 14 to 3 (1956, 1971, and 2011) and leads to strongly amplified (factors 4–10) and statistically significant reductions in PPT, carbon uptake, ET, and environmental stresses through the entire year (Table 2, column 4; Figure 3, cyan). JULES shows stronger negative TER anomalies compared to previously discussed ENSO/NAO conditions, but the ratio of anomalies of NEP to GPP increases from 24% in the first case (ENSO/NAO < 0) to 33% in the present case, indicating an increasing impact of low water availability and GPP loss on regional carbon uptake and conversion of TexMex to net carbon source in every season except autumn. These anomalies are some of the largest in TexMex over the last 63 years (Figure 4), with 2011 ranking as one of the largest anomalies in North America over the last 30 years [*Zscheischler et al.*, 2014a]. Given the significance of these anomalies relative to climatology and year-to-year variability, it appears likely that increasing severity of La Niña during negative phases of NAO has led to significant reductions in carbon uptake on at least three different occasions since 1950 tied to enhanced soil moisture and heat stress.

Finally, we sort events based by strong NAO (NAO $< -1\sigma$) and La Niña (ENSO $< -1\sigma$) years and find that only the 2011 drought matches this criteria. In other words, 2011 represents the only year in the 63 year climatology that negative phases of NAO and ENSO both exceed -1σ, where the NAO $= -1.61$ exceeds -2σ (second largest event on record next to 2010 after filtering) and ENSO $= -1.38$ exceeds -1σ (seventh largest event on record). This climatologically rare event leads to further amplification of all anomalies. JULES shows especially high PPT deficits in winter and spring which, unlike normal ENSO/NAO < 0 years, extends well into summer and fall (Figure 3a, red line). This exceeds climatological variability by 2σ, precipitation loss in ENSO $< -1\sigma$ and NAO < 0 years by 40%, and precipitation loss in ENSO/NAO < 0 years by an order of magnitude.

Spring and summer precipitation deficits in 2011 were strongly amplified relative to ENSO/NAO < 0 years and the most extreme over the 63 year record (Figure 4a). This had extreme effects on environmental stress indicators, including directly producing negative SoilW anomalies and indirectly producing positive SWdwn and Ts anomalies (through decreased cloudiness), the latter two of which also approach their highest anomalies on record. Effects on ecosystem function include highest negative anomalies of GPP ($-0.50\,\mathrm{Pg\,C\,yr^{-1}}$), ET ($-0.42\,\mathrm{kg\,m^{-2}\,s^{-1}}$), and NEP ($-0.23\,\mathrm{Pg\,C\,yr^{-1}}$) on record (see Figure 4 and Table 2, column 6), and third highest anomaly of LAI ($-0.085\,\mathrm{m^2\,m^{-2}}$). The ratio of simulated NEP to GPP loss also increases to 45% in 2011, such that GPP loss drives a 50% increase in CO_2 flux to the

atmosphere, likely due to record high temperatures (1 K warmer on average) and relative increase in heterotrophic respiration, consistent with findings by *Rajan et al*. [2013].

Given the extreme nature of the 2011 drought relative to the 1950–2012 climatology, we repeat our analysis excluding 2011 to test for robustness. In general, we find similar spatial patterns of precipitation in Figure 1 but with fewer significant grid points, including elimination of significant grid points in south and east Texas in ENSO < 0 years (Figure 1a) and in north Texas in ENSO/NAO < 0 years (Figure 1c). While removal of 2011 leads to a reduction in the magnitude of negative anomalies at seasonal scale and a loss of significance for NEP, the negative anomalies of PPT, GPP, and ET retain their significance throughout the entire year for ENSO $< -1\sigma$ and NAO < 0 years (Table 2, column 5). These results support our primary finding that strong La Niña years and negative NAO years have led to significant impairments of ecosystem function.

In summary, model simulations constrained by observed climate show that hot, dry, and sunny conditions associated with strong La Niña's and exacerbated by negative phases on the NAO lead to climatologically significant reductions of carbon uptake in the TexMex regions, with impacts to GPP ($-312\,\mathrm{g\,C\,m^{-2}\,yr^{-1}}$ or $-0.42 \pm 0.18\,\mathrm{Pg\,C\,yr^{-1}}$) representing one third of typical TexMex gross productivity ($1.3\,\mathrm{Pg\,C\,yr^{-1}}$) and impacts to NEP ($-103$ g C m $^{-2}$ yr^{-1} or $-0.14 \pm 0.11\,\mathrm{Pg\,C\,yr^{-1}}$) causing a carbon neutral region to become a significant carbon source. This drought-induced carbon source is amplified under extremely warm temperatures such as during the 2011 drought due to smaller decreases in heterotrophic respiration relative to GPP.

3.4 Evaluation of JULES Carbon Fluxes During 2011 TexMex Drought

Estimates of GPP constrained satellite SIF observations (GOPT) show decreased GPP throughout TexMex during TMD11 (Figure 5a). From GOPT, we estimate a total annual GPP reduction of $0.42 \pm 0.04\,\mathrm{Pg\,C\,yr^{-1}}$ in the TexMex domain, representing a 37% decrease in GPP from 2010 ($1.13\,\mathrm{Pg\,C\,yr^{-1}}$) to 2011 ($0.70\,\mathrm{Pg\,C\,yr^{-1}}$), with strongest reductions in central and eastern Texas (Figure 5a). This GPP decrease is strongest in semiarid ecosystems (0.60 Pg C for JULES and 0.34 Pg C for IGBP) and driven primarily by grasslands (0.28 Pg C and 0.19 Pg C, respectively). GPP is reduced throughout the year (Figure 5c, solid) but most significantly in the growing season, with a slight recovery or increase of GPP at the end of the year in late fall/early winter. SIF is also reduced in 2011 (Figure 5c, dashed) but only by half as much as GOPT, reflecting a combination of enhanced a priori constraint (higher agreement among eight biosphere models) and reduced observational constraint (assimilation of fewer SIF data). Cross marks indicate grid points where ΔGOPT exceeds posterior uncertainty and hence where GOPT tendencies are determined to be statistically significant. Assimilation of satellite SIF strongly reduces prior uncertainty from the

ensemble of eight TRENDY models and produces significant GPP reductions in the eastern portions of Texas and Oklahoma.

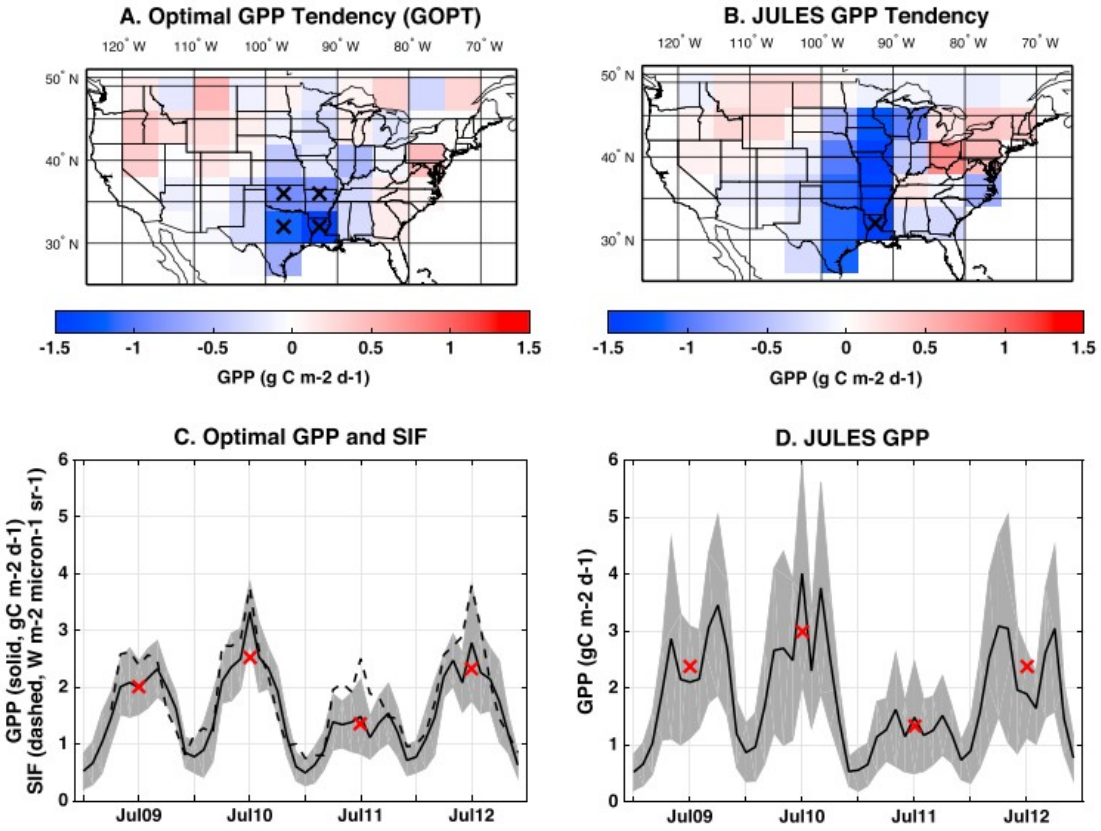

Figure 5. Gross primary production (GPP) tendencies from 2010 to 2011 for (a and c) SIF constrained GPP (GOPT) and (b and d) model GPP (JULES). Maps (Figures 5a and 5b) are calculated as the annual mean difference from 2011 to 2010 (blue shading represents less GPP in 2011), where cross marks indicate grid points where GPP tendencies in JULES and GOPT exceed prior and posterior uncertainty, respectively. Time series (Figures 5c and 5d) represent monthly GPP (solid) and solar-induced chlorophyll fluorescence (SIF) from 2009 to 2012 averaged across the TexMex study region, indicated by the black boxes in Figures 5a and 5b. Red crosses are the growing season (Apr–Sep) average. Shading represents GPP uncertainty.

The geographic distribution of JULES GPP tendencies in 2011 is consistent with GOPT throughout TexMex (Figures 5a and 5b). However, JULES GPP reductions, estimated as $0.63 \pm 0.09\,\mathrm{Pg\,C\,yr^{-1}}$ (0.50 Pg C semiarid) from 2010 ($1.34\,\mathrm{Pg\,C\,yr^{-1}}$) to 2011 ($0.71\,\mathrm{Pg\,C\,yr^{-1}}$), exceed GOPT ($0.42 \pm 0.04\,\mathrm{Pg\,C\,yr^{-1}}$) by nearly 50% in the TexMex region, largely due to higher-simulated GPP during the 2010 growing season (Figure 5d). High uncertainty of JULES GPP tendencies is driven by high spread among eight biosphere models in this region (fewer cross marks in Figure 5b and higher-uncertainty range in 2011 in Figure 5d). A model intercomparison study of carbon flux sensitivity to climate extremes shows similar high spread across model ensembles but general agreement of GPP loss during drought [*Zscheischler et al.*, 2014b].

JULES shows a fairly wide range of negative GPP tendencies throughout TexMex, with increasing magnitude of GPP loss from west to east. This spatial pattern is highly consistent with GOPT, and the high slope ($y = 1.5x +$

0.026) supports the findings above, indicating a 50% greater GPP variability in JULES. The high correlation ($r = 0.91 \pm 0.17$, $p = 0.0015$) is encouraging but expected given the use of JULES as a prior in the GOPT estimation methodology. Thus, we also check for consistency against independent estimates from the flux tower-based MPI and reflectance based MOD17. Comparison to MPI indicates high correlation of GPP tendencies ($r = 0.84 \pm 0.22$, $p = 0.0097$) but factor of 2 stronger variability ($y = 1.9x - 0.073$). Comparison to MOD17 shows reduced correlation of GPP tendencies ($r = 0.43 \pm 0.37$, $p = 0.29$) but improved agreement of GPP variability ($y = 1.2x - 0.12$). In all cases, model and semiempirical products show GPP loss in all TexMex grid points. In general, these comparisons show consistency of spatial patterns and a likely overestimate of GPP loss.

Eddy covariance observations show consistent patterns of decreasing CO_2 uptake across Texas and New Mexico in 2011 relative to 5+ year averages from 2005 to 2012 in Texas and 2007 to 2012 in New Mexico (Table 1 and Figure 6). NEP decreases (less CO_2 uptake) across all sites relative to both the previous year and the 5+ year average and thus represents a potentially significant departure from the long-term average. NEP increases slightly at first at the beginning of the year but decreases quickly during the growing season (~April–September) and into autumn. We also find simultaneous decreases in GPP and TER during drought, consistent with experiments [*Shi et al.*, 2014] and other observational studies [*Law et al.*, 2001; *Ciais et al.*, 2005; *Schwalm et al.*, 2010, 2012]. NEP reductions due to reduced canopy photosynthesis are slightly offset by NEP increases by suppressed microbial respiration. While these processes have competing effects on ecosystem carbon sink capacity, the GPP effect is larger and thus primarily responsible for the reduced NEP in 2011. Growing season NEP reduction averaged across towers is $144\ \mathrm{g\ C\ m^{-2}}$ relative to 2010, about half of that observed in northern Texas over the same period [*Rajan et al.*, 2013], and $82\ \mathrm{g\ C\ m^{-2}}$ relative to the multiyear average (based on the average of available months and extrapolated annually).

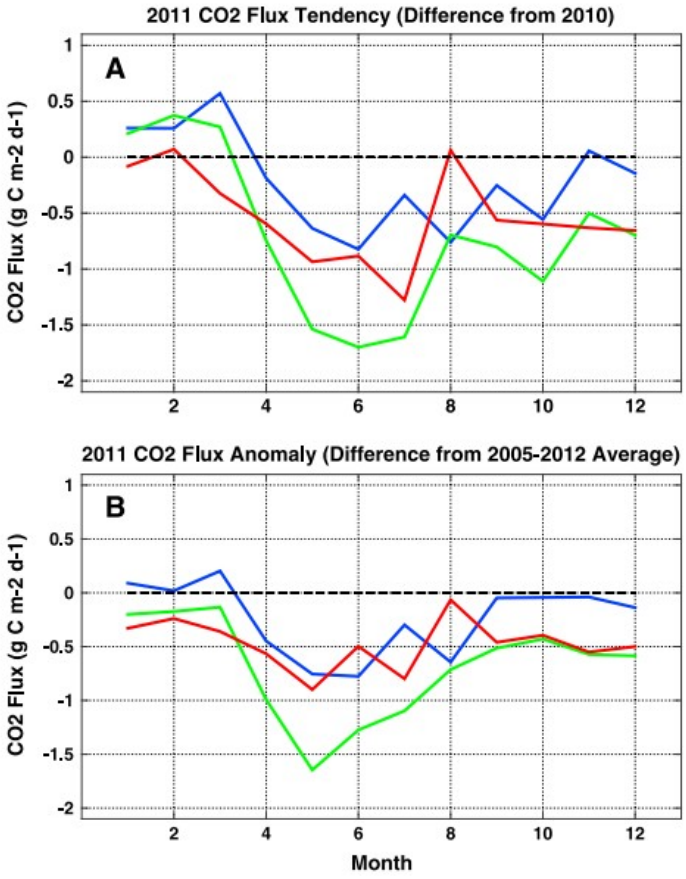

Figure 6. Monthly gross and net CO_2 flux anomalies averaged across five eddy covariance towers in TexMex, including gross primary production (GPP, green), terrestrial ecosystem respiration (TER, red), and net ecosystem production (NEP, blue). (a) Values in flux tendencies (difference of 2011 from 2010); (b) flux anomalies (difference from 5+ year average based on available data from 2005 to 2012 in Texas and 2007 to 2012 in New Mexico). Negative values denote a reduction of CO_2 flux in 2011.

Comparison of JULES 2011 CO_2 flux anomalies to the five flux tower sites analyzed here shows highly consistent patterns of GPP, TER, and NEP reductions across TexMex (Figure 7). We find high correlation of negative GPP anomalies ($r = 0.92 \pm 0.23$, $p = 0.027$) with increasing GPP reductions from west to east and highest GPP loss in southern Texas (represented by FR2). JULES GPP variability is roughly 33% that observed from flux towers ($y = 0.36x - 0.15$). We note that JULES GPP tendencies are unique for each flux tower despite identical sampling of JULES grid boxes for two different sets of flux towers (Mpj/Vcm and Vcp/Wjs) which are geographically close in proximity. Differences in JULES GPP tendencies for these locations arise due to different flux tower sampling times, record length, and coarse model spatial scale.

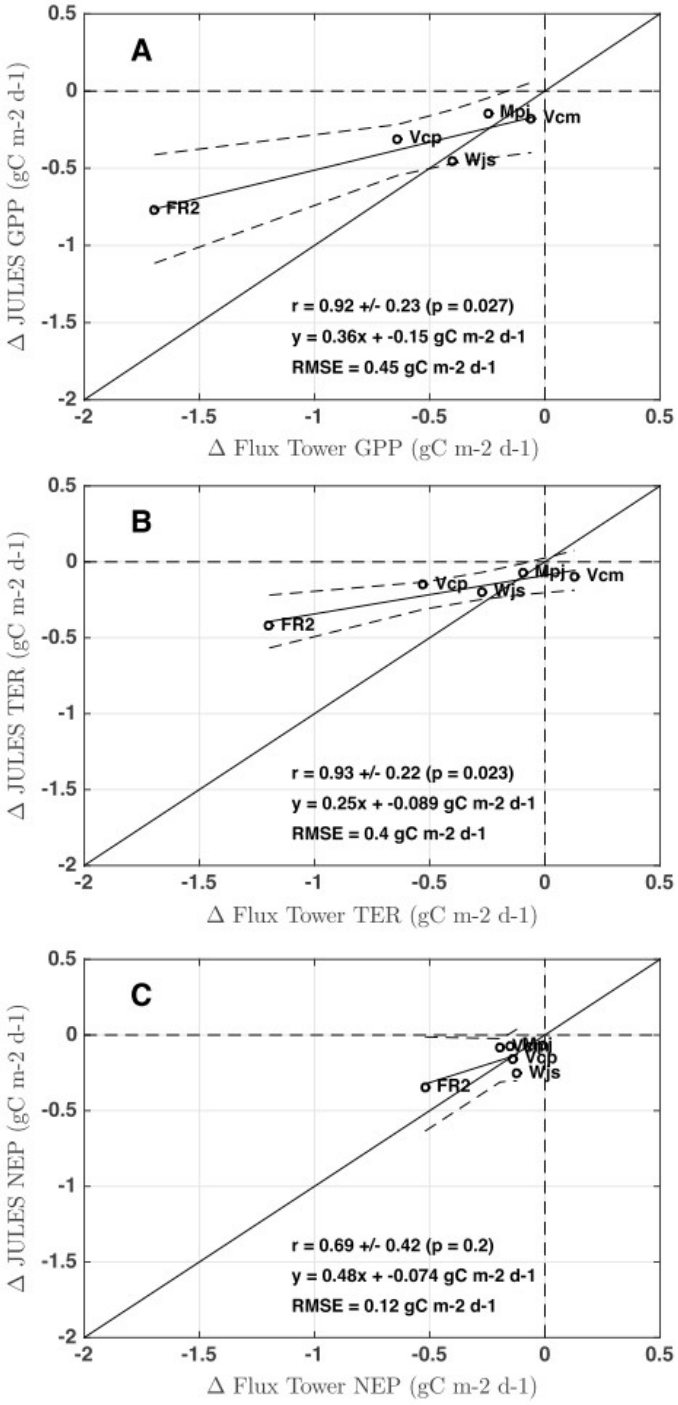

Figure 7. Regressions of annual CO_2 flux anomalies (difference of 2011 from 5+ year average) of JULES onto flux tower anomalies for (a) gross primary production (GPP), (b) terrestrial ecosystem respiration (TER), and (c) net ecosystem production (NEP). Model GPP is sampled at the same time as flux towers and in the grid cell closest to the tower location. Correlation (r), p value (p), slope/y intercept (y), and root-mean-square error are also shown.

Negative TER anomalies in JULES are also highly correlated with flux towers ($r = 0.93 \pm 0.22$, $p = 0.023$) and significantly smaller (25%) than observed ($y = 0.25x - 0.089$). In theory, a significant difference between GPP and TER in

either of these statistics could lead to NEP predictions that are inconsistent with observations, such that a model correctly predicts component fluxes but fails to reproduce the net flux. However, JULES shows a similar low bias for both GPP and TER anomalies (33% and 25% of observed, respectively). Since JULES simulates consistent ranges of variability for component fluxes including stronger GPP loss, it also captures observed patterns of NEP loss at all sites ($r = 0.69 \pm 0.42$, $p = 0.2$) and with a smaller overall bias than component fluxes ($y = 0.48x - 0.074$).

Our model evaluation of carbon flux changes during TMD11 provides high confidence that JULES simulates spatial patterns of GPP reductions across TexMex with high fidelity. We note, however, that the magnitude of JULES estimates has a high bias compared to estimates constrained at similar scales by remote sensing observations. We can adjust simulated estimates assuming the 50% high bias implied by our regional remote sensing observational analysis and assuming the low bias relative to flux towers is related to scale mismatches. In this case, expected reductions during the three major drought events from 1950 to 2012 (1956, 1971, and 2011) associated with strong La Niña's and negative NAO's are more likely closer to $-208\,\mathrm{g\,C\,m^{-2}\,yr^{-1}}$ for GPP and $-69\,\mathrm{g\,C\,m^{-2}\,yr^{-1}}$ for NEP. These adjusted losses are highly consistent with carbon uptake losses observed at FLUXNET eddy covariance sites in grassland and woody savannah ecosystems in western North America during a long-term drought from 2000 to 2004, including a total GPP loss of $-177\,\mathrm{g\,C\,m^{-2}\,yr^{-1}}$ and NEP loss of $-69\,\mathrm{g\,C\,m^{-2}\,yr^{-1}}$ [cf. *Schwalm et al*., 2012, Figure 3]. These results suggest that linkages of TexMex carbon uptake to variability of ENSO and the NAO have played a major role in carbon uptake variability in North America over the recent historical record.

3.5 Evaluation of JULES Water Fluxes During 2011 TexMex Drought

Satellite observations show widespread decreases in soil moisture in 2011 (Figure 8). In particular, SMOS indicates decreases in surface soil moisture throughout southern and middle portions of North America, with peak loss in east Texas (Figure 8a) and a 40% decrease from 2010 to 2011 in TexMex (Figure 8c). GRACE also shows widespread decreases in total column water in similar regions as SMOS, with peak loss in central Texas (Figure 8b). However, negative tendencies in GRACE tend to decrease more gradually moving outward from central Texas than is apparent in SMOS, indicating more spatial variability in the soil moisture response to drought than in total column water. Satellite soil moisture tendencies in TexMex are highly consistent with predicted total soil moisture (SoilW) reductions in JULES, with a correlation of SMOS/JULES tendencies of $r = 0.94 \pm 0.14$ ($p = 0.0005$) and GRACE/JULES tendencies of 0.71 ± 0.29 ($p = 0.046$). Observed soil moisture is also highly correlated with semiempirical GPP reductions (Figure 9) with correlation of SMOS/GOPT tendencies of $r = 0.82 \pm 0.23$ ($p = 0.12$; Figure 9a) and GRACE/GOPT tendencies of $r = 0.92 \pm 0.16$ ($p = 0.0013$; Figure 9b).

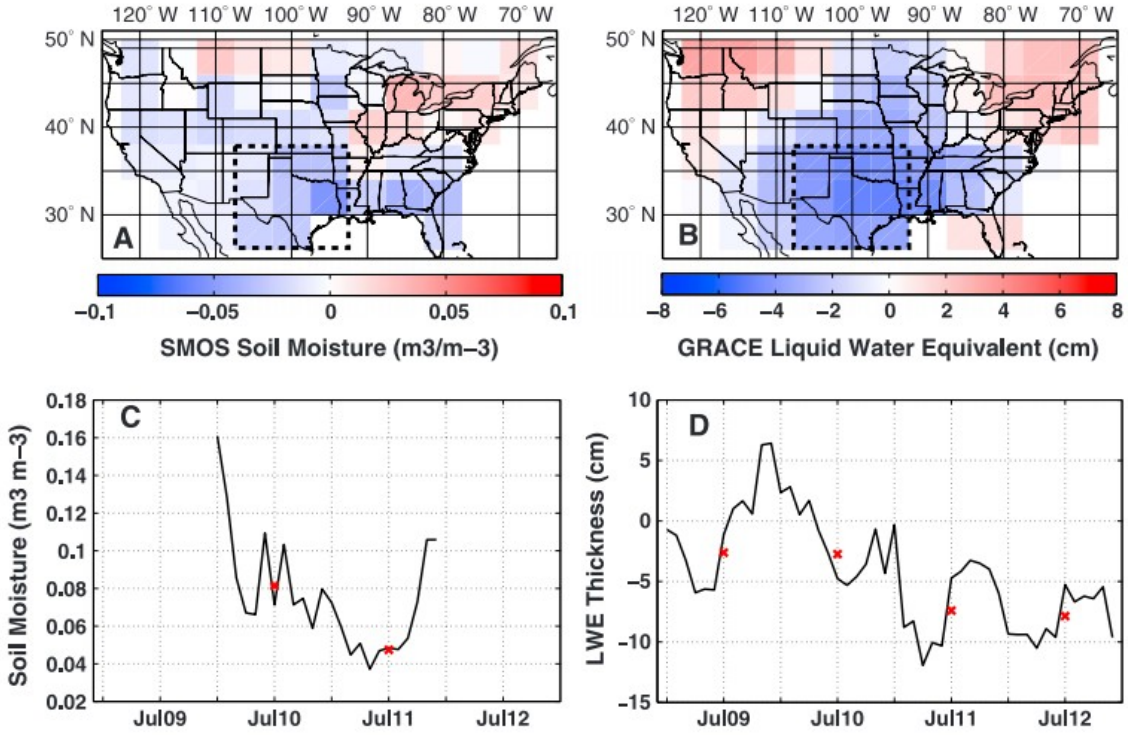

Figure 8. Soil moisture tendencies from 2010 to 2011 for SMOS and GRACE. (a and b) Maps are calculated as the annual mean difference from 2011 to 2010 (blue shading represents lower values in 2011). (c and d) Time series represent monthly soil moisture from 2009 to 2012 averaged across the TexMex study region, indicated by the black boxes in Figures 8a and 8b. Red crosses are the growing season (Apr–Sep) average.

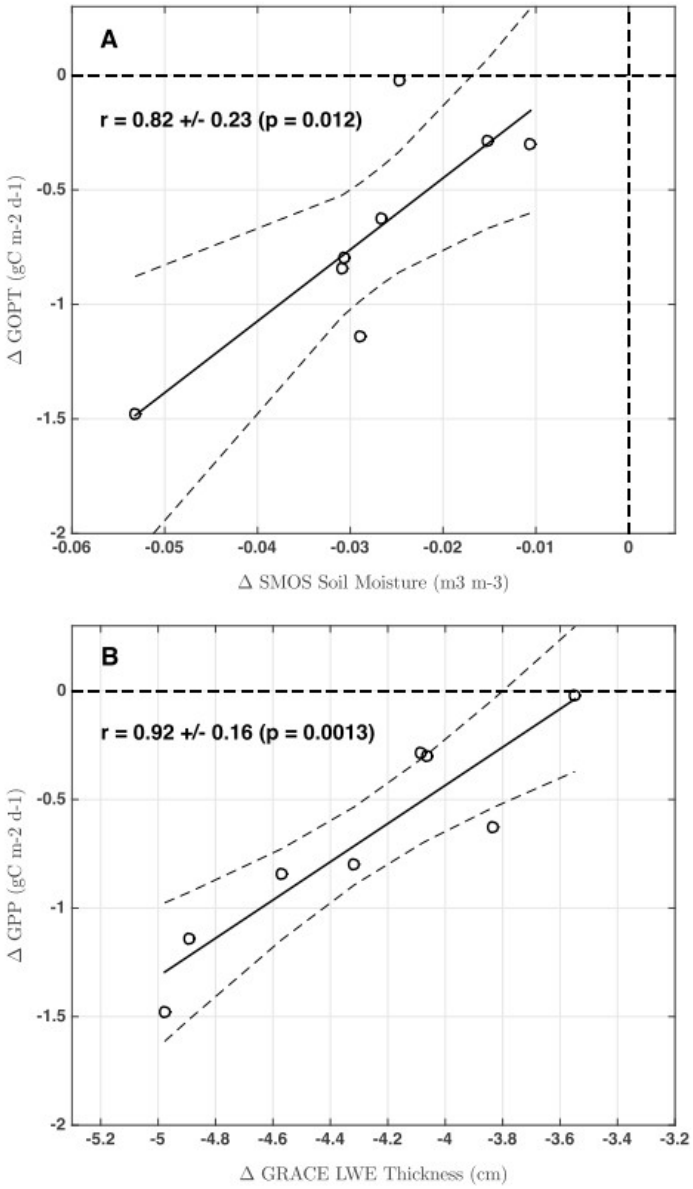

Figure 9. Regressions of regional mean annual 2011 tendencies (difference of 2011 from 2010) of GOPT onto (a) SMOS soil moisture and (b) GRACE liquid water equivalent (LWE), respectively. Correlation and *p* value are also shown.

The combination of CO_2 flux and soil moisture data from satellites and flux towers provides convincing empirical evidence, supporting our JULES simulations of decreasing carbon uptake across semiarid ecosystems of TexMex driven by soil water stress during concurrent negative phases of ENSO and NAO. These results are consistent with key findings by *Zscheischler et al*. [2014a, 2014c] that drought and low water availability are the main cause for regional GPP loss across the planet including the TexMex region.

4 Conclusions

We have used a robust model-observational analysis over the period 1950–2012 to capture a clear relationship between climate variability, drought, and carbon uptake in semiarid ecosystems of the Texas-northern Mexico region (i.e., TexMex). Increasing intensity of overlapping negative phases of ENSO and the NAO leads to systematic impairment of ecosystem function, including significantly reduced biological uptake of CO_2 and reduced flux of groundwater to the atmosphere. JULES predictions of carbon uptake reductions during the 2011 record drought fall within the range of estimates from remote sensing and flux tower data in the region, with an overestimate of carbon uptake reductions relative to remote sensing-based estimates and an underestimate relative to flux towers. Predictions of the sign and spatial distribution of 2011 carbon flux (GPP, TER, and NEP) and soil moisture (surface and deep) anomalies are highly consistent with ground-based and remote sensing observations.

Future La Niña's and negative NAO's are likely to continue to reduce the capacity of semiarid ecosystems in the southern Great Plains to absorb CO_2 and emit water, and projected drying and increasing intensity and frequency of droughts in this region will exacerbate these effects [*Seneviratne et al*., 2012; *Collins et al*., 2013; *Walsh et al*., 2014]. However, the magnitude of these effects in future climates is confounded by several other processes happening in parallel, including future CO_2 fertilization, which is expected to increase water use efficiency through partial stomata closure and consequently increase the rate of carbon uptake per unit of water lost [*Morgan et al*., 2011; *Keenan et al*., 2013; *Xu et al*., 2013; *Zscheischler et al*., 2014d], and increasing fractional vegetation, which will increase total carbon assimilation in semiarid ecosystems [*Donohue et al*., 2013]. Future studies should therefore examine the expected carbon and water cycle responses of the TexMex region to La Niña and the NAO under future climate projections with and without elevated CO_2 and with a special focus on grasslands which dominate the region.

The ability to predict the carbon-climate feedbacks in response to future La Niña's depends fundamentally on atmospheric model fidelity in representing ENSO, the NAO, and associated changes in precipitation. While these atmospheric patterns show up in observational analyses, coupled ocean-atmosphere simulations, including those from phase 5 of the Coupled Model Intercomparison Project (CMIP5), strongly underestimate the intensity of the 2011 Texas-Mexico drought [*Hoerling et al*., 2013; *Seager et al*., 2014] and hence the magnitude of carbon uptake reductions. Even when these models are driven by prescribed sea surface temperatures, they fail to represent the spatial patterns and magnitudes of precipitation in North America [*Hoerling et al*., 2013]. This is attributed partly to model inability to simulate the NAO as well as the extreme difficulty in modeling precipitation and is likely to lead to biases in carbon cycle projections from CMIP5 models [e.g., *Ahlström et al*., 2012]. Results from this study highlight a need to improve atmospheric model predictions of ENSO and the NAO in order to improve predictions of

future impacts on the carbon cycle and the associated feedbacks to climate change.

Acknowledgments

CRU-NCEP climate information is obtained from ftp://nacp.ornl.gov/synthesis/2009/frescati/model_driver/cru_ncep/analysis/readme.htm. ENSO and NAO indices are obtained at NOAA CPC (http://www.cpc.ncep.noaa.gov/products/analysis_monitoring/ensostuff/ensoyears.shtml). JULES model output and CRU-NCEP data are provided by A. Harper (A.Harper@exeter.ac.uk). SMOS data are available for data access at http://catds.ifremer.fr/Products/Products-access. Chlorophyll fluorescence data were provided by C. Frankenberg (Christian.Frankenberg@jpl.nasa.gov). MPI-BGC data set was provided by M. Jung (martin.jung@bgc-jena.mpg.de). MODIS MOD17 GPP data are available at http://www.ntsg.umt.edu/project/mod17. GRACE land data are available at http://grace.jpl.nasa.gov. Flux tower data are collected/processed by M. Litvak (marcy.litvak@gmail.com) and gap-filled/partitioned by S. Wolf (sewolf@berkeley.edu). We acknowledge all MODIS land product science team members for providing an invaluable public data set. The improved MOD17 GPP data were provided by the Numerical Terradynamic Simulation Group at the University of Montana. We thank the Global Carbon Project and TRENDY modelers for contributing model output. We also give special thanks to S. Sitch and P. Friedlingstein for organizing TRENDY. GRACE land data processing algorithms were provided by S. Swenson and supported by the NASA MEaSUREs Program. SMOS data were obtained from the Centre Aval de Traitement des Données SMOS (CATDS), operated for the Centre National d'Etudes Spatiales (CNES, France) by IFREMER (Brest, France). S. Wolf acknowledges support from a Marie Curie International Outgoing Fellowship. T.F. Keenan acknowledges support from a Macquarie University Research Fellowship. M. Litvak acknowledges support from NASA ROSES Program. We give special thanks to A. Mialon for providing assistance in the processing and interpretation of the SMOS data set. This research was funded by the NASA Atmospheric CO_2 Observations from Space (ACOS) program (grant NNX10AT42G) and carried out at the Jet Propulsion Laboratory, California Institute of Technology, under a contract with NASA © 2014.

References

Ahlström, A., G. Schurgers, A. Arneth, and B. Smith (2012), Robustness and uncertainty in terrestrial ecosystem carbon response to CMIP5 climate change projections, *Environ. Res. Lett.*, 7, 044008, 1– 9.

Anderson-Teixera, K. J., J. P. DeLong, A. M. Fox, D. Brese, and M. E. Litvak (2011), Climate change will reduce the capacity of Southwest ecosystems to sequester and store carbon, *Global Change Biol.*, 17, 410– 424.

Barnston, A. G., and R. E. Livezey (1987), Classification, seasonality and persistence of low frequency atmospheric circulation patterns, *Mon. Weather Rev.*, 115, 1083– 1126.

Beer, C., et al. (2010), Terrestrial gross carbon dioxide uptake: Global distribution and covariation with climate, *Science*, 329, 834– 838.

Best, M. J., et al. (2011), The Joint UK Land Environment Simulator (JULES), model description—Part 1: Energy and water fluxes, *Geosci. Model Dev.*, 4, 677– 699, doi:10.5194/gmd-4-677-2011.

Ciais, P., et al. (2005), Europe-wide reduction in primary productivity caused by the heat and drought in 2003, *Nature*, 437(7058), 529– 533.

Clark, D. B., et al. (2011), The Joint UK Land Environment Simulator (JULES), model description—Part 2: Carbon fluxes and vegetation dynamics, *Geosci. Model Dev.*, 4, 701– 722, doi:10.5194/gmd-4-701-2011.

Colby, B., and P. Tanimoto (2011), in *Using Climate Information to Improve Electric Utility Load Forecasting. Adaptation and Resilience: The Economics of Climate-Water-Energy Challenges in the Arid Southwest*, edited by B. G. Colby and G. B. Frisvold, pp. 207– 228, RFF Press, Washington, D. C.

Collatz, G. J., J. T. Ball, C. Grivet, and J. A. Berry (1991), Physiological and environmental regulation of stomatal conductance, photosynthesis and transpiration: A model that includes a laminar boundary layer, *Agric. For. Meteorol.*, 54, 107– 136.

Collatz, G. J., M. Ribas-Carbo, and J. A. Berry (1992), Coupled photosynthesis-stomatal conductance model for leaves of C_4 plants, *Aust. J. Plant Physiol.*, 19, 519– 538.

Collins, M., et al. (2013), Long-term climate change: Projections, commitments and irreversibility, in *Climate Change 2013: The Physical Science Basis. Contribution of Working Group I to the Fifth Assessment Report of the Intergovernmental Panel on Climate Change*, edited by T. F. Stocker et al., pp. 1029– 1136, Cambridge Univ. Press, Cambridge, U. K., and New York.

Cox, P. M. (2001), Description of the TRIFFID Dynamic Global Vegetation Model, Hadley Centre Technical Note 24, Hadley Centre, Met Office, Bracknell, U. K.

Cox, P. M., C. Huntingford, and R. J. Harding (1998), A canopy conductance and photosynthesis model for use in a GCM land surface scheme, *J. Hydrol.*, 213, 79– 94.

Cox, P. M., R. A. Betts, C. D. Jones, S. A. Spall, and I. J. Totterdell (2000), Acceleration of global warming due to carbon-cycle feed- backs in a coupled climate model, *Nature*, 408, 184– 187.

Craine, J. M., J. B. Nippert, A. J. Elmore, A. M. Skibbe, S. L. Hutchinson, and N. A. Brunsell (2012), Timing of climate variability and grassland productivity, *Proc. Natl. Acad. Sci. U.S.A.*, 109(9), 3401– 3405.

Daumard, F., S. Champagne, A. Fournier, Y. Goulas, A. Ounis, J.-F. Hanocq, and I. Moya (2010), A field platform for continuous measurement of canopy fluorescence, *IEEE Trans. Geosci. Remote Sens.*, 48, 3358.

Donohue, R. J., M. L. Roderick, T. R. McVicar, and G. D. Farquhar (2013), Impact of CO_2 fertilization on maximum foliage cover across the globe's warm, arid environments, *Geophys. Res. Lett.*, 40, 3031– 3035, doi:10.1002/grl.50563.

Efron, B. (1979), Bootstrap methods: Another look at the jackknife, *Ann. Stat.*, 7, 1– 26.

Essery, R. L. H., M. J. Best, R. A. Betts, P. M. Cox, and C. M. Taylor (2003), Explicit Representation of Subgrid Heterogeneity in a GCM Land Surface Scheme, *J. Hydrometeor.*, 4, 530– 543.

Fannin, B. (2012), Updated 2011 Texas agricultural drought losses total $7.62 billion, Agrilife Today.

Frankenberg, C., et al. (2011), New global observations of the terrestrial carbon cycle from GOSAT: Patterns of plant fluorescence with gross primary productivity, *Geophys. Res. Lett.*, 38, L17706, doi:10.1029/2011GL048738.

Hoerling, M., A. Kumar, R. Dole, J. W. Nielsen-Gammon, J. Eischeid, J. Perlwitz, X.-W. Quan, T. Zhang, P. Pegion, and M. Chen (2013), Anatomy of an extreme event, *J. Clim.*, 26, 2811– 2832.

Hurrell, J. W., and C. Deser (2009), North Atlantic climate variability: The role of the North Atlantic Oscillation, *J. Mar. Syst.*, 78(1), 28– 41.

Jacobs, C. M. J. (1994), *Direct Impact of Atmospheric CO2 Enrichment on Regional Transpiration*, pp. 1– 179, Wageningen Agricultural Univ., Netherlands.

Jacquette, E., A. Al Bitar, A. Mialon, Y. H. Kerr, A. Quesney, F. Cabot, and P. Richaume (2010), SMOS CATDS level 3 global products over land, *Proc. SPIE*, 7824, doi:10.1117/12.865093.

Jung, M., et al. (2011), Global patterns of land-atmosphere fluxes of carbon dioxide, latent heat, and sensible heat derived from eddy covariance, satellite, and meteorological observations, *J. Geophys. Res.*, 116, G00J07, doi:10.1029/2010JG001566.

Keenan, T. F., D. Y. Hollinger, G. Bohrer, D. Dragoni, J. W. Munger, H. P. Schmid, and A. D. Richardson (2013), Increase in forest water-use efficiency as atmospheric carbon dioxide concentrations rise, *Nature*, 499, 324– 327.

Kerr, Y. H., et al. (2010), The SMOS Mission: New tool for monitoring key elements of the global water cycle, *Proc. IEEE*, 98(5), 666– 687.

King, A. W., et al. (2015), North America's net terrestrial CO2 exchange with the atmosphere 1990–2009, *Biogeosciences*, 12, 399– 414.

Knapp, A. K., et al. (2002), Rainfall variability, carbon cycling, and plant species diversity in a mesic grassland, *Science*, 298, 2202– 2205, doi:10.1126/science.1076347.

L'Heureux, M. L., D. C. Collins, and Z.-Z. Hu (2012), Linear trends in sea surface temperature of the tropical Pacific Ocean and implications for the El Niño-Southern Oscillation, *Clim. Dyn.*, 40, 1223– 1236, doi:10.1007/s00382-012-1331-2.

Landerer, F. W., and S. C. Swenson (2012), Accuracy of scaled GRACE terrestrial water storage estimates, *Water Resour. Res.*, 48, W04531, doi:10.1029/2011WR011453.

Law, B., F. Kelliher, D. Baldocchi, P. Anthoni, J. Irvine, D. V. Moore, and S. Van Tuyl (2001), Spatial and temporal variation in respiration in a young ponderosa pine forest during a summer drought, *Agric. For. Meteorol.*, 110(1), 27– 43.

LeComte, D. (2012), International weather highlights 2011: Flood and famine, *Weatherwise*, 65, 28– 33, doi:10.1080/00431672.2012.670076.

Lee, J. E., et al. (2013), Forest productivity and water stress in Amazonia: Observations from GOSAT chlorophyll fluorescence, *Proc. R. Soc. B, Biol. Sci.*, 280(1761), 9.

Long, D., B. R. Scanlon, L. Longuevergne, A. Y. Sun, D. N. Fernando, and H. Save (2013), GRACE satellite monitoring of large depletion in water storage in response to the 2011 drought in Texas, *Geophys. Res. Lett.*, 40, 3395–3401, doi:10.1002/grl.50655.

Morgan, J. A., D. R. LeCain, E. Pendall, D. M. Blumenthal, B. A. Kimball, Y. Carrillo, D. G. Williams, J. Heisler-White, F. A. Dijkstra, and M. West (2011), C4 grasses prosper as carbon dioxide eliminates desiccation in warmed semi-arid grassland, *Nature*, 476(7359), 202– 205.

Myneni, R. B., et al. (2007), Large seasonal swings in leaf area of Amazon rainforests, *Proc. Natl. Acad. Sci. U.S.A.*, 104, 4820– 2823.

Myoung, B., and J. W. Nielsen-Gammon (2010), The convective instability pathway to warm season drought in Texas. Part I: The role of convective inhibition and its modulation by soil moisture, *J. Clim.*, 23, 4461– 4473.

Namias, J. (1991), Spring and summer 1988 drought over the contiguous United States—Causes and prediction, *J. Clim.*, 4, 54– 65.

Nigam, S., B. Guan, and A. Ruiz-Barradas (2011), Key role of the Atlantic Multidecadal Oscillation in 20th central drought and wet periods over the Great Plains, *Geophys. Res. Lett.*, 38, L16713, doi:10.1029/2011GL048650.

Parazoo, N. C., K. Bowman, J. B. Fisher, C. Frankenberg, D. B. A. Jones, A. Cescatti, Ó. Pérez-Priego, G. Wohlfahrt, and L. Montagnani (2014), Terrestrial gross primary production inferred from satellite fluorescence and vegetation models, *Global Change Biol.*, 20, 3103– 3121, doi:10.1111/gcb.12652.

Rajan, N., S. J. Maas, and S. Cui (2013), Extreme drought effects on carbon dynamics of a semiarid pasture, *Agron. J.*, 105(6), 1749– 1760.

Reichstein, M., et al. (2013), Climate extremes and the carbon cycle, *Nature*, 500(7462), 287– 295.

Running, S. W., R. R. Nemani, F. A. Heinsch, M. Zhao, M. Reeves, and H. Hashimoto (2004), A continuous satellite-derived measure of global terrestrial primary production, *BioScience*, 54(6), 547– 560.

Schwalm, C. R., et al. (2010), Assimilation exceeds respiration sensitivity to drought: A fluxnet synthesis, *Global Change Biol.*, 16(2), 657– 670.

Schwalm, C. R., C. A. Williams, and K. Schaefer (2011), Carbon consequences of global hydrologic change, 1948–2009, *J. Geophys. Res.*, 116, G03042, doi:10.1029/2011JG001674.

Schwalm, C. R., C. A. Williams, K. Schaefer, D. Baldocchi, T. A. Black, A. H. Goldstein, B. E. Law, W. C. Oechel, K. T. Paw U, and R. L. Scott (2012), Reduction in carbon uptake during turn of the century drought in western North America, *Nat. Geosci.*, 5(8), 551– 556.

Seager, R., L. Goddard, J. Nakamura, N. Henderson, and D. E. Lee (2014), Dynamical causes of the 2010/11 Texas-Northern Mexico Drought, *J. Hydrometeorol.*, 15(1), 39– 68.

Sellers, P. J. (1985), Canopy reflectance, photosynthesis and transpiration, *Int. J. Remote Sens.*, 6(8), 1335– 1372.

Sellers, P. J., et al. (1997), Modeling the exchanges of energy, water, and carbon between continents and the atmosphere, *Science*, 275, 502– 509.

Seneviratne, S. I., T. Corti, E. L. Davin, M. Hirschi, E. B. Jaeger, I. Lehner, B. Orlowsky, and A. J. Teuling (2010), Investigating soil moisture-climate interactions in a changing climate: A review, *Earth Sci. Rev.*, 99, 125– 161.

Seneviratne, S. I., et al. (2012), Changes in climate extremes and their impacts on the natural physical environment, in *Managing the Risks of Extreme Events and Disasters to Advance Climate Change Adaptation, A Special Report of Working Groups I and II of the Intergovernmental Panel on Climate Change (IPCC)*, edited by C. B. Field et al., pp. 109– 230, Cambridge Univ. Press, Cambridge, U. K., and New York.

Shafer, M., D. Ojima, J. M. Antle, D. Kluck, R. A. McPherson, S. Petersen, B. Scanlon, and K. Sherman (2014), *Great Plains. Climate Change Impacts in the United States: The Third National Climate Assessment*, edited by J. M. Melillo, T. (. T. C.). Richmond, and G. W. Yohe, chap. 19, pp. 441– 461, U.S. Global Change Research Program, Washington, D. C., doi:10.7930/J0D798BC.

Shi, H., L. Li, D. Eamus, J. Cleverly, A. Huete, J. Beringer, Q. Yu, E. van Gorsel, and L. Hutley (2014), Intrinsic climate dependency of ecosystem light and water-use-efficiencies across Australian biomes, *Environ. Res. Lett.*, 9, 104002, 12.

Sitch, S., et al. (2015), Recent trends and drivers of regional sources and sinks of carbon dioxide, *Biogeosciences*, 12(3), 653– 679.

Smith, A. B., and R. W. Katz (2013), US billion-dollar weather and climate disasters: Data sources, trends, accuracy and biases, *Nat. Hazards*, 67(2), 387– 410.

Swenson, S. C., and J. Wahr (2006), Post-processing removal of correlated errors in GRACE data, *Geophys. Res. Lett.*, 33, L08402, doi:10.1029/2005GL025285.

Tapley, B. D., S. Bettadpur, J. C. Ries, P. F. Thompson, and M. M. Watkins (2004), GRACE measurements of mass variability in the Earth system, *Science*, 305(5683), 503– 505, doi:10.1126/science.1099192.

U.S. Department of Agriculture (2014), Atlas of Rural and Small-Town America. U.S. Department of Agriculture Economic Research Service. [Available at http://www.ers.usda.gov/data-products/atlas-of-rural-and-small-town-america/go-to-the-atlas.aspx.]

Walsh, J., et al. (2014), *Our Changing Climate. Climate Change Impacts in the United States: The Third National Climate Assessment*, edited by J. M. Melillo, T. (. T. C.). Richmond, and G. W. Yohe, chap. 2, pp. 19– 67, U.S. Global Change Research Program, Washington, D. C., doi:10.7930/J0KW5CXT.

Xiao, J., et al. (2011), Assessing net ecosystem carbon exchange of U.S. terrestrial ecosystems by integrating eddy covariance flux measurements and satellite observations, *Agric. For. Meteorol*, 151(1), 60– 69.

Xu, Z., H. Shimizu, Y. Yagasaki, S. Ito, Y. Zheng, and G. Zhou (2013), Interactive effects of elevated CO_2, drought, and warming on plants, *J. Plant Growth Regul.*, 32(4), 692– 707.

Zscheischler, J., M. Reichstein, S. Harmeling, A. Rammig, E. Tomelleri, and M. D. Mahecha (2014a), Extreme events in gross primary production: A characterization across continents, *Biogeosciences*, 11, 2909– 2924.

Zscheischler, J., et al. (2014b), Impact of large-scale climate extremes on biospheric carbon fluxes: An intercomparison based on MsTMIP data, *Global Biogeochem.Cycles*, 28, 585– 600, doi:10.1002/2014GB004826.

Zscheischler, J., et al. (2014c), A few extreme events dominate global interannual variability in gross primary production, *Environ. Res. Lett.*, 9, 035001, doi:10.1088/1748-9326/9/3/035001.

Zscheischler, J., M. Reichstein, J. von Buttlar, M. Mu, J. T. Randerson, and M. D. Mahecha (2014d), Carbon cycle extremes during the 21st century in

CMIP5 models: Future evolution and attribution to climatic drivers, *Geophys. Res. Lett.*, 41, 8853– 8861, doi:10.1002/2014GL062409.